The Suckling Hills Fault, Kayak Island Zone, and accretion of the Yakutat microplate, Alaska

James B. Chapman,[1,2] Lindsay L. Worthington,[3] Terry L. Pavlis,[1] Ronald L. Bruhn,[4] and Sean P. Gulick[5]

Received 13 May 2011; revised 3 October 2011; accepted 12 October 2011; published 13 December 2011.

[1] The Suckling Hills and Kayak Island are isolated mountain blocks located along strike from each other within the foreland of the St. Elias orogen in southern Alaska. These blocks preserve an erosional surface that was deformed by slip on northwest-dipping reverse faults in the Pleistocene. We suggest that the Suckling Hills Fault and Kayak Island Zone form a segmented fault network that links with the Bering Glacier structure to the north. This fault network separates the central Yakataga fold and thrust belt from complex, multiply deformed structures in the western syntaxis. Ongoing accretion of the Yakutat microplate to North America results in translation of structures of the fold and thrust belt into the western syntaxis. The composite Suckling Hills Fault, Kayak Island Zone, and Bering Glacier structure may have formed because the older structures of the fold and thrust belt were unfavorably oriented within the western syntaxis region. This pattern of deformation provides a template for understanding the complex deformation within the core of the western syntaxis and predicts refolding and straightening of the western syntaxis margin with continued accretion. This study provides an analog for structural overprinting and changing deformation patterns through time in orogenic corners.

Citation: Chapman, J. B., L. L. Worthington, T. L. Pavlis, R. L. Bruhn, and S. P. Gulick (2011), The Suckling Hills Fault, Kayak Island Zone, and accretion of the Yakutat microplate, Alaska, *Tectonics*, *30*, TC6011, doi:10.1029/2011TC002945.

1. Introduction

[2] The Yakutat microplate converges with the south Alaska margin at 4–5 cm/yr to form the St. Elias orogen [*Plafker*, 1987; *Elliott et al.*, 2010]. Because of the arcuate geometry and obliquity of the St. Elias convergence zone, the orogen contains multiple structural domains along strike [*Bruhn et al.*, 2004]. East of the Malaspina Glacier, the orogen consists of an eastern structural domain dominated by right-lateral strike-slip fault systems and narrow forethrusts [*Bruhn et al.*, 2004] (Figure 1). Between the Malaspina Glacier and the Bering Glacier is the central Yakataga Fold and Thrust Belt (YFTB), which is a thin-skinned, predominantly dip-slip, series of thrust sheets [*Meigs et al.*, 2008; *Bruhn et al.*, 2004] (Figure 1). West of the Bering Glacier, the Yakutat microplate subducts at a low angle beneath North America. This structural domain is characterized by complex deformational overprints related to a corner geometry and formation of an incipient syntaxis [*Bruhn et al.*, 2004, *Pavlis et al.*, 2004] (Figure 1). For this study, we examine the structural domain boundary between the central YFTB and this syntaxis, hereafter referred to as the western syntaxis. Detailed investigation of this syntaxis is intended to increase understanding of the process of structural overprinting and evolving deformation through time in orogenic corners.

[3] The boundary between the central YFTB and the western syntaxis consists of a series of parallel-trending faults zones found along strike that include the Bering Glacier structure [*Bruhn et al.*, 2010; *Doser et al.*, 2007], the Kayak Island Zone [*Plafker*, 1987; *Worthington et al.*, 2008], and the lesser known Suckling Hills Fault. We build upon previous studies that have individually examined the structural importance of these structures [*Worthington et al.*, 2008; *Bruhn et al.*, 2010; *Plafker*, 1987] and suggest that these structures form a single, segmented fault network bordering the eastern margin of the western syntaxis (Figure 2). This fault network may form the northeastern extension of the Aleutian megathrust as it transitions from the North America-Pacific Plate boundary to the Yakutat-North America microplate boundary [*Worthington et al.*, 2008; *Bruhn et al.*, 2004; *Eberhart-Phillips et al.*, 2006].

[4] Researchers have hypothesized that this boundary accommodates some component of convergence between the Yakutat microplate and North America [*Plafker et al.*, 1994; *Bruhn et al.*, 2010]. However, whether these structures are recently active remains unanswered. To this end, we investigate deformed geomorphic markers off of Kayak Island and in the Suckling Hills and demonstrate that the Kayak Island Zone-Suckling Hills fault network has been active in the

[1]Department of Geological Sciences, University of Texas at El Paso, El Paso, Texas, USA.
[2]Now at SandRidge Energy, Oklahoma City, Oklahoma, USA.
[3]Department of Geology and Geophysics, Texas A&M University, College Station, Texas, USA.
[4]Department of Geology and Geophysics, University of Utah, Salt Lake City, Utah, USA.
[5]Institute for Geophysics, University of Texas at Austin, Austin, Texas, USA.

0278-7407/11/2011TC002945

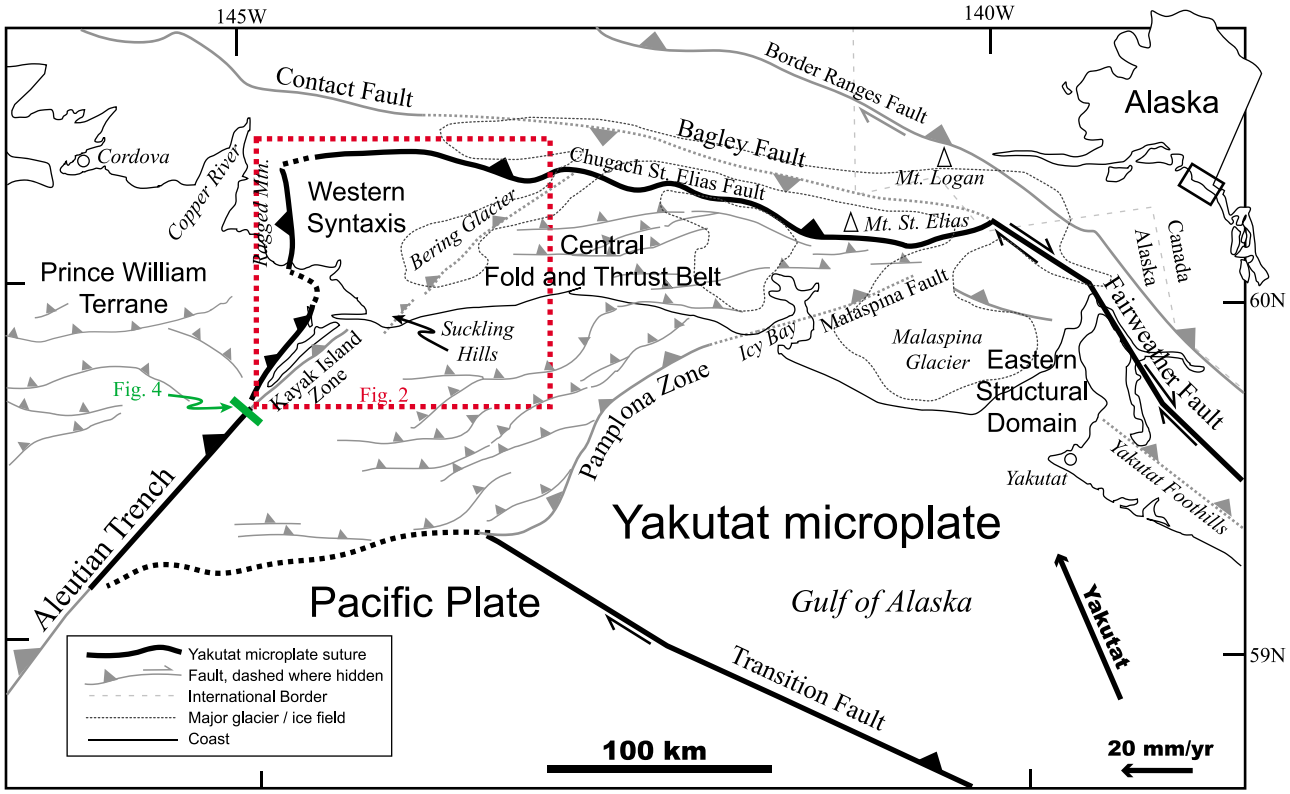

Figure 1. Tectonic map of the Yakutat microplate showing fault geometries and structural domains across the orogen including the central Yakataga Fold and Thrust Belt and the western syntaxis. Fault locations from *Pavlis et al.* [2004]. Yakutat microplate velocity from *Elliott et al.* [2010].

Pleistocene. We combine these data with structural observations and suggest that this young fault network has refolded and structurally overprinted older fold and thrust structures of the central YFTB that were translated into the western syntaxis. Finally, we discuss the tectonic evolution of the western syntaxis margin and present a model of continuous accretion, refolding, and straightening of the margin with time.

2. Geologic Setting

[5] The Yakutat microplate consists of a single, thick, oceanic plateau basement assemblage [*Christeson et al.*, 2010; L. L. Worthington et al., Crustal structure of the Yakutat terrane: New constraints for understanding the evolution of subduction and collision in southern Alaska, submitted to *Journal of Geophysical Research*, 2011] and several kilometers of early Eocene and younger sedimentary cover [*Plafker*, 1987]. Since the mid-Cenozoic, the Yakutat microplate has traveled northward relative to North America with the basement assemblage subducted beneath central Alaska [*Eberhart-Phillips et al.*, 2006] and the sedimentary cover stripped off to form the YFTB [*Plafker*, 1987]. The sedimentary cover is readily divided between pretectonic strata including the Kultheith, Token, Stillwater, and Poul Creek formations that are mid-Eocene to earliest Miocene in age, and syntectonic strata of the Miocene to present Yakataga formation [*Plafker*, 1987]. The Yakataga formation is diachronous across the St. Elias orogen with a general decrease in age to the east [*Lagoe et al.*, 1993; *Plafker and Addicott*, 1976]. At Kayak Island, the basal Yakataga Formation is believed to be late Miocene in age based on molluscan biostratigraphy [*Plafker and Addicott*, 1976] and a 6 Ma pluton that intrudes the Yakataga Formation on the southern end of the island [*Plafker*, 1974] (Figure 2).

[6] Characteristic of the central YFTB are gently plunging folds trending approximately east–west that strike oblique to the current Yakutat microplate motion [*Elliott et al.*, 2010] (Figure 2). In contrast to the approximately east–west structural trend of the central YFTB, the western syntaxis contains numerous mountain blocks with a structural grain dominated by north–south to northeast-southwest striking bedding, axial planes, and faults [*Miller*, 1961, 1975] (Figure 2). The orientation of these structures is sub-perpendicular to Yakutat plate motion direction [*Elliott et al.*, 2010] and sub-parallel to the Pamplona Zone and Malaspina Fault, which form the leading deformation front for the YFTB (Figure 1).

[7] Previous studies of the western syntaxis reveal areas where the northeasterly striking bedding, axial surfaces, and fault planes are wrapped around fold axes that plunge moderately to steeply toward the northwest [*Bruhn et al.*, 2004; *Pavlis and Bruhn*, 2011]. *Bruhn et al.* [2004] considered these younger folds superimposed on an older fold-thrust system. To the northwest, in the core of the western syntaxis, these overprints become increasingly complex, including a large-scale, northwest trending antiform that deforms the older fold-thrust system and possibly the suture between the Yakutat microplate and the Mesozoic Prince William accretionary complex [*Pavlis et al.* 2004; *Pavlis and Bruhn*, 2011]. These complex structures are absent east of the

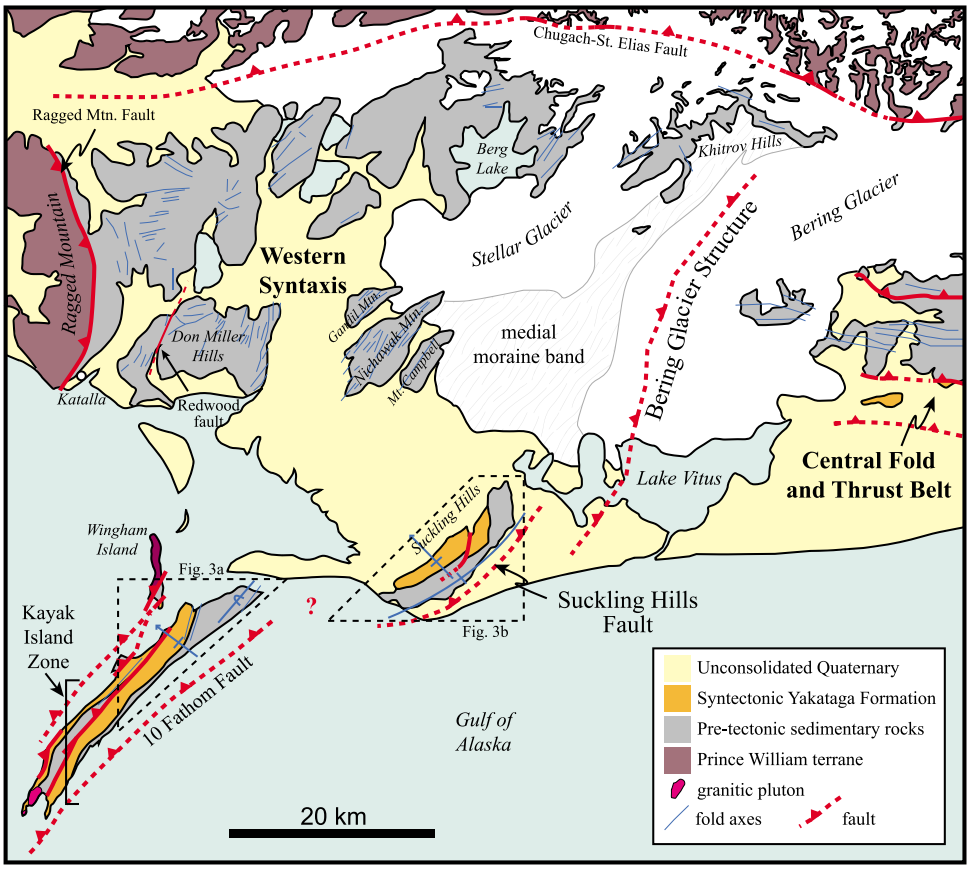

Figure 2. Map of the western syntaxis area showing major structures and Bering-Stellar glacial system. The Kayak Island Zone, Suckling Hills Fault, and Bering Glacier structure form the eastern boundary of the western syntaxis. Fold axes are shown in blue. Faults are dashed where hidden. Geology compiled by *Richter et al.* [2005]. Location shown in Figure 1.

Kayak Island Zone, Suckling Hills Fault, and Bering Glacier structure. In this study, we examine these three fault segments as a combined fault system that defines the boundary of the western syntaxis, extending from the Aleutian Trench to the Chugach-St. Elias Fault (Figure 1).

[8] The Kayak Island Zone consists of several steeply dipping to overturned reverse faults, the westernmost of which is the Yakutat microplate suture [*Plafker*, 1974; *Worthington et al.*, 2008] (Figure 2). The leading fault, on the southeastern side of the Kayak Island Zone is the Ten Fathom Fault, which is defined by a bathymetric scarp [*Plafker*, 1974] (Figure 2). Like the faults, bedding at Kayak Island is sub-vertical to overturned, with tops to the northwest [*Plafker*, 1974] (Figure 3a). The steep bedding is related to continued rotation in the hanging wall of the northeast-striking reverse faults *Plafker* [1974]. A recently published high-resolution seismic line across the southern end of Kayak Island images the upper few kilometers of the offshore Kayak Island Zone [*Worthington et al.*, 2008] and is analyzed as part of this study to constrain fault geometries, compare geomorphic features, and estimate slip rates (Figure 4). Northeast of the Kayak Island Zone is the Suckling Hills Fault, which was first shown in a compilation map by *Richter et al.* [2005], but the details of the fault including the geometry and deformation history remain unresolved. The Bering Glacier structure is inferred from earthquake relocations, structural relationships, and glacial dynamics [*Doser et al.*, 2007; *Bruhn et al.*, 2010]. Geophysical studies near Kayak Island and the Suckling Hills suggest that, locally, the basal décollement beneath the sedimentary cover is located at ~15 km depth and dips northwest beneath the YFTB at 5–6 degrees [*Griscom and Sauer*, 1990; *Brocher et al.*, 1994; *Eberhart-Phillips et al.*, 2006; *Jaeger et al.*, 1998]. This décollement intersects the surface ~100 km east of Kayak Island at the Pamplona Zone, the offshore limit to active deformation within the YFTB [*Plafker*, 1987; *Worthington et al.*, 2008, 2010] (Figure 1).

[9] Yakutat-North America convergence is accommodated by a combination of structures west of the Malaspina Glacier, although quantification of deformation across specific structures is difficult. Restoration of sections drawn from seismic interpretations suggests that the Pamplona Zone currently absorbs 10–15% of the convergence between the Yakutat microplate and North America [*Chapman et al.*, 2008; *Worthington et al.*, 2010]. Other offshore YFTB structures between the Pamplona Zone and Kayak Island Zone are overlapped by Pleistocene sediments and not considered active [*Bruns and Schwab*, 1983; *Worthington et al.*, 2008; *Berger et al.*, 2008]. As a result of these analyses, a large fraction of Yakutat-North America convergence remains unaccounted for. Some of the remaining strain is transferred into the Alaskan interior [*Mazzotti and Hyndman*,

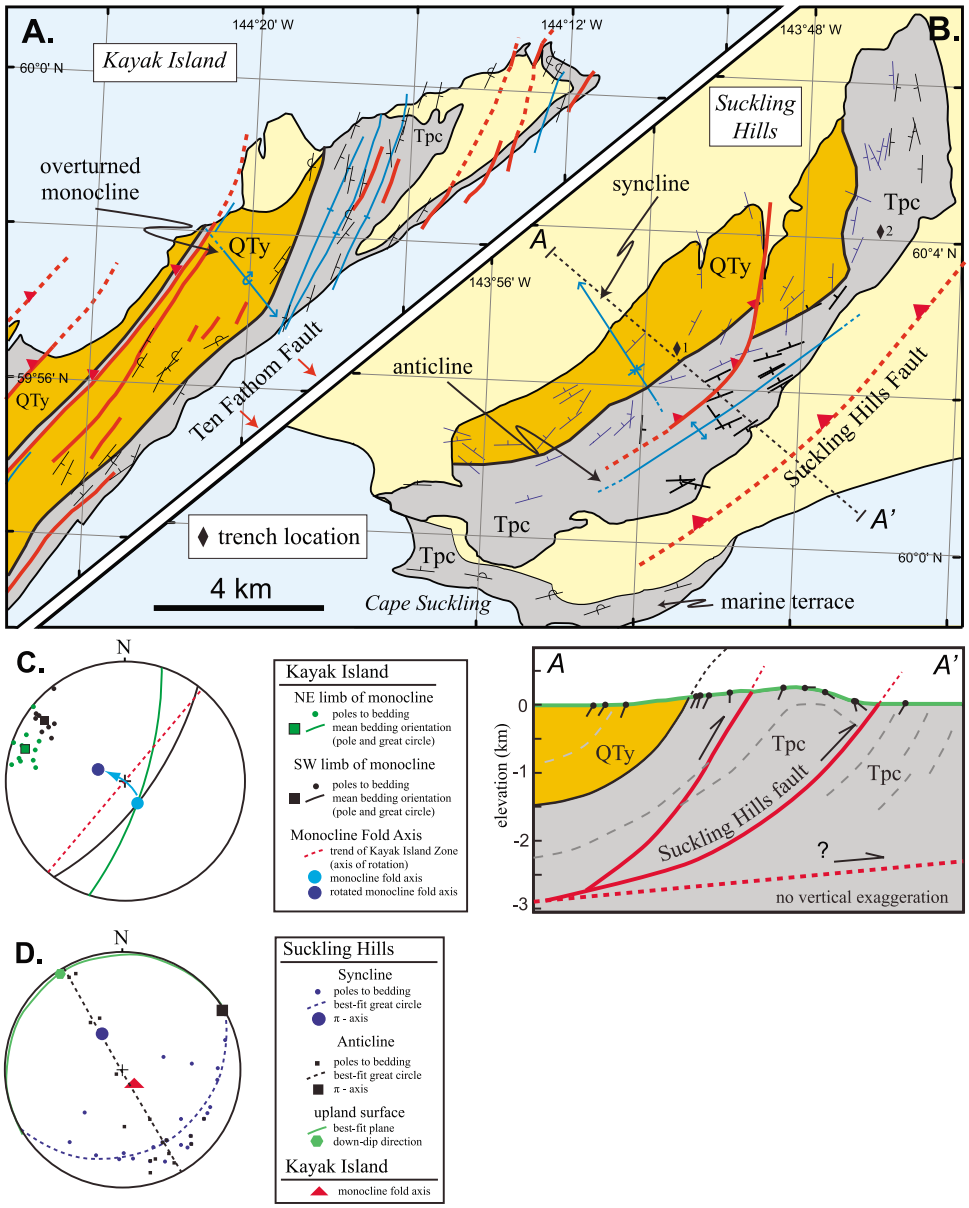

Figure 3. Structural geology of the Suckling Hills and Kayak Island. Fold axes shown in blue, unconsolidated Quaternary deposits shown in pale yellow. Location of maps shown in Figure 2. (a) Geologic map of Kayak Island after *Plafker* [1974]. (b) Geologic map of the Suckling Hills and associated cross-section. In the cross-section, dashed lines are bedding traces and ball and stick data points represent projected structural data. Fault geometry is constrained by bedding relationships and comparisons to the Kayak Island Zone along strike. Thin (∼2 m) loess deposits are not shown, see Figure 6 for outline. (c) Equal area stereonet plot of the limbs, fold axis, and partially restored and rotated fold axis of the monocline exposed on Kayak Island. (d) Equal area stereonet plot of structural elements of the Suckling Hills and Kayak Island. Blue circles correspond to blue strike and dip symbols and black squares correspond to bold strike and dip symbols in Figure 3b.

2002], but many researchers hypothesize that the western syntaxis area could accommodate some component of motion [*Bruhn et al.* 2004; *Pavlis et al.*, 2004; *Plafker et al.*, 1994]. *Plafker* [1987] considered the Kayak Island Zone active, however, *Worthington et al.* [2008] identified undeformed seafloor sediments across the southern Kayak Island Zone and near vertical bedding within the fault zone suggesting an incipient suture. *Bruhn et al.* [2010] have hypothesized that the Bering Glacier structure may be active, although activity is obscured by the Bering Glacier. A cluster of very young AHe ages (∼.5 Ma) west of the Bering Glacier suggest rapid exhumation, although it is difficult to separate a possible tectonic signal from glacial erosion [*Berger and Spotila*, 2008]. Although there are no assessments of active slip across the Suckling Hills Fault, *Plafker* [1969] recorded anomalously high coseismic uplift (4–5 m) in the 1964

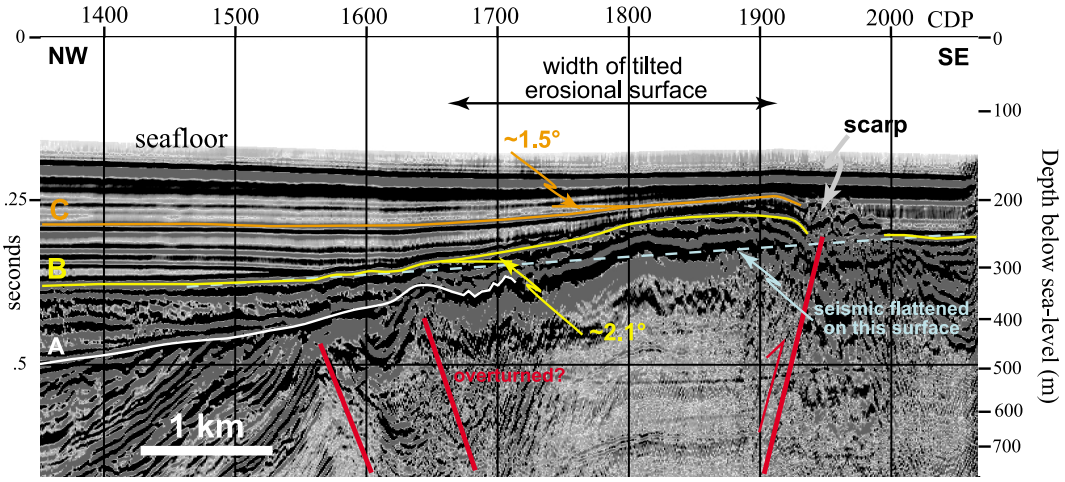

Figure 4. High-resolution seismic profile across the southern Kayak Island Zone, adapted from *Worthington et al.* [2008]. Fault interpretation and interpretation of Horizon A and Horizon B from *Worthington et al.* [2008]. Location of the seismic profile is shown in Figure 1.

Alaska earthquake, which he suggested may be related to local faulting or warping.

3. Glacial History

[10] Geomorphic surfaces resulting from glacial advances provide both timing and geometric markers that allow us to constrain slip histories. In the vicinity of the Suckling Hills and Kayak Island, the Cordilleran Ice sheet reached its Last Glacial Maximum (LGM) and began to retreat at ~14.5 ka [*Chapman et al.*, 2009; *Sirkin and Tuthill*, 1987; *Denton*, 1974; *Rymer and Sims*, 1982]. Peat deposits near Katalla suggest ice had retreated past the present coastline by ~10 ka [*Fleisher et al.*, 1999] and had reached its present position by 9.3–9.6 ka [*Hamilton*, 1994]. Glacial advances older than the LGM are not well documented onshore within the Yakutat microplate, but regional data from southern Alaska suggest the penultimate glaciation occurred at 50–60 ka [*Briner and Kaufman*, 2008] with the next oldest glacial advance at ~140 ka [*Briner and Kaufman*, 2008; *Begét*, 2001]. A regional angular unconformity on the continental shelf is linked to the Mid-Pleistocene Transition (0.7–1 Ma), which is the oldest glacial advance to have crossed the entire extent of the orogenic belt [*Berger et al.*, 2008; *Worthington et al.*, 2008; *Clark et al.*, 2006]. This unconformity may mark a transition from smaller, dispersed glacial termini to more erosive, concentrated ice streams because it predates the development of younger unconformities associated with modern sea-valleys [*Berger et al.*, 2008; *Worthington et al.*, 2008]. For this study, we consider the Mid-Pleistocene Transition a maximum potential age for the geomorphic surfaces observed in the Kayak Island Zone and Suckling Hills. There are no known geomorphic surfaces in the onshore portion of the YFTB with age estimates as old as, or older than, the Mid-Pleistocene Transition.

4. Data and Analysis

[11] We seek to characterize the Kayak Island Zone and Suckling Hills Fault as part of a young, potentially active, fault network bordering the western syntaxis that originated as older structures of the central YFTB were translated into the western syntaxis area. For this purpose, we have analyzed structural data and identified deformed, erosional surfaces at Kayak Island and the Suckling Hills that we interpret as evidence of recent fault activity. Our data set combines previously recorded structural data [*Plafker*, 1974; *Worthington et al.*, 2008; *Richter et al.*, 2005; *Miller*, 1961, 1975] and results from our own field work as part of the St. Elias Erosion and Tectonics Project (STEEP) including new optically stimulated luminescence (OSL) ages. OSL samples were processed at the Utah State University Luminescence lab following procedures detailed by *Rittenour et al.* [2005]. For the Kayak Island Zone, we depth converted a portion of the high-resolution seismic profile GOA-3002, originally presented by *Worthington et al.* [2008], using a smoothed velocity scaled from stacking velocities (Figure 4). This profile crosses the Kayak Island Zone approximately 20 km off the southwestern tip of Kayak Island (Figure 1). For the Suckling Hills, we generated a 15 m resolution digital elevation model (DEM) from stereoscopic very near infrared (VNIR) bands within an advanced spaceborne thermal emission and reflection radiometer (ASTER) image, which we used to aid in the identification and study of the erosional surface.

4.1. The Kayak Island Zone

[12] At the northeastern end of Kayak Island, a monocline is exposed with a fold axis plunging 73 degrees toward 150 and an interlimb angle of 161 degrees (Figures 3a and 3c). The monocline is defined by a change in the strike of bedding from a NE-SW strike on the southwestern limb of the monocline to a NNE-SSW strike on the northeastern limb. Bedding is near vertical to overturned in both limbs of the monocline. Bedding relationships and the plunge direction of the monocline fold axis suggest that the monocline is overturned by rotation in the hanging wall of the Ten Fathom Fault or a similarly oriented reverse fault. The Ten Fathom Fault is located ~2.5 km east of the coast of Kayak Island and is only known from seismic and bathymetric surveys

[*Plafker*, 1974] (Figure 2). For comparison to folds in the Suckling Hills in the following sections, we perform a partial restoration of the Kayak Island Zone by rotating overturned bedding in the monocline around a horizontal axis parallel to the trend of the Kayak Island Zone (040 degrees) (Figure 3c). The analysis rotates the fold axis of the monocline until it is plunging 70 degrees, resulting in a trend of 293. We chose a plunge of 70 degrees as an arbitrary cut-off for the restoration. This partial restoration rotates overturned bedding in the hanging wall of the Ten Fathom Fault into an upright, but still steeply dipping position. While not a full restoration, the partial restoration illustrates the general trend of the monocline fold axis prior to becoming overturned. Also present on Kayak Island are a series of shallowly plunging folds with axes trending 020 to 045, sub-perpendicular to the trend of the monocline fold axis and parallel to the strike of the steeply dipping reverse faults (Figure 3a). The overturned monocline and the shallowly plunging folds represent two separate generations of folds, consistent with other areas in the western syntaxis.

4.2. The Kayak Island Offshore Surface

[13] The offshore Kayak Island Zone consists of at least three major faults including a large reverse fault at the southeastern end of the fault zone that dips 60 $\pm$ 10 degrees to the northwest and may be the Ten Fathom Fault of *Plafker* [1974] (Figure 4). The other faults shown in Figure 4 dip toward the southeast at 50–70 degrees and may be back thrusts or could be overturned reverse faults, similar to some faults observed on the surface. These faults are truncated and eventually overlapped by flat-lying sediments at the seafloor.

[14] Horizon B from *Worthington et al.* [2008] is an erosional unconformity that separates more steeply dipping beds of the Yakataga formation below from lesser deformed sediments above (Figure 4). Older erosional unconformities are present lower in the seismic profile including Horizon A from *Worthington et al.* [2008], however, we did not detect any other unconformities above Horizon B (Figure 4). Partial chronologies exist for the Yakutat shelf sediments east of Kayak Island [*Zellers*, 1995; *Berger et al.*, 2008], but we were unable to tie them directly into the Kayak Island section. Regional relationships, including comparison with offshore seismic profiles south of the Bering Glacier [*Berger et al.*, 2008; *Worthington et al.*, 2008], suggest that the unconformity associated with Horizon B in the Kayak Island Zone was likely produced by glacial advance onto the shelf and could be as old as the Mid-Pleistocene Transition (0.7–1 Ma) [*Clark et al.*, 2006; *Berger et al.*, 2008] or as young as the LGM ($\sim$14.5 ka). Above Horizon B, sediments are deformed across the top of the Kayak Island Zone in what we interpret as a backlimb to the leading northwest dipping fault (Figure 4). These sediments reach a maximum thickness of $\sim$180 m along the seismic line, which is consistent with Holocene sediment thickness estimates of 100–150 m for the area west of Kayak Island [*Carlson and Molnia*, 1975]. Holocene sediment accumulation rates west of Kayak Island are 1–2 cm/yr [*Jaeger et al.*, 1998]. We use these accumulation rates to back-calculate an approximate age range for Horizon B that leads us to favor a LGM age for Horizon B. Older unconformities preserved below Horizon B, including Horizon A, may be related to older glaciations, although additional research is needed (Figure 4).

[15] Across the Kayak Island Zone, Horizon B dips to the northwest at $\sim$2 degrees (Figure 4). Tilt of overlying beds progressively decreases upsection to an undeformed seafloor. Whereas some of the shallowest reflectors are characterized by depositional onlap of strata, many reflectors thin toward the Kayak Island Zone and others are visibly deformed across the top of the Kayak Island Zone (Figure 4). West of the Kayak Island Zone, for example, Horizon C is $\sim$70 m below the seafloor and appears to slope upwards to be as little as 20 m below the seafloor across the top of the Kayak Island Zone with a dip of $\sim$1 degree (Figure 4). The decrease in dip from Horizon B to Horizon C is likely related to differential compaction [*Carminati and Santantonio*, 2005] and progressive rotation in the hanging wall of the fault. Above Horizon C, flat-lying sediments overlap the Kayak Island Zone, which *Worthington et al.* [2008] interpret as an indication of waning deformation across the Kayak Island Zone (Figure 4). The apparently flat-lying sediments above Horizon C could also reflect a low rotation rate that is not easily interpreted in the youngest part of the section.

[16] A scarp with $\sim$30 m offset separates tilted reflectors above Horizon B in the hanging wall of the leading fault from the base of flat-lying sediments in the footwall of the fault to the southeast (Figure 4). Assuming that the Horizon B unconformity formed at the LGM ($\sim$14.5 ka), offset across the scarp suggests $\sim$2.1 mm/yr vertical uplift and a slip rate of $\sim$2.4 mm/yr using a 60 degree dip on the fault.

4.3. The Suckling Hills

[17] The Suckling Hills contain many of the same structural characteristics as Kayak Island, located along strike. First, the Suckling Hills Fault bounds the Suckling Hills in the same structural position as the Ten Fathom Fault off Kayak Island. Second, like Kayak Island, bedding in the Suckling Hills dips steeply (60 to 70 degrees) to the northwest (Figure 3b) suggesting a similar orientation for the Suckling Hills Fault at depth. Third, the two fault blocks contain the same stratigraphic assemblage, including the contact between the Yakataga and Poul Creek Formations. Finally, and perhaps most significantly, both the Suckling Hills and Kayak Island record two generations of folding.

[18] Two map-scale folds are present in the Suckling Hills, a broad, open syncline with a fold axis plunging 61 degrees toward 330 and an open anticline with a fold axis plunging 2 degrees toward 060 across the length of the Suckling Hills (Figures 3b and 3d). The trends of the twofold axes are perpendicular to each other suggesting multiple phases of deformation, consistent with other areas in the western syntaxis. The anticline is positioned at the easternmost edge of the Suckling Hills and oriented parallel to the Suckling Hills Fault, consistent with a fault-bend fold or fault-propagation fold in the hanging wall of the fault (Figure 3b). Bedrock exposures in the footwall of the Suckling Hills Fault are limited to isolated outcrops of Poul Creek Formation in the Suckling Hills marine terrace. Bedding in these locations dips steeply (60 degrees to vertical) and strikes 090 to 110 degrees at the marine terrace to the west and 070 to 075 degrees along the coast to the east (Figure 3b). Facing indicators are limited to relatively ambiguous graded beds, however, our work concurs with *Miller* [1961] who suggested bedding is generally upright and north facing. Additional research is needed to determine if the Suckling Hills

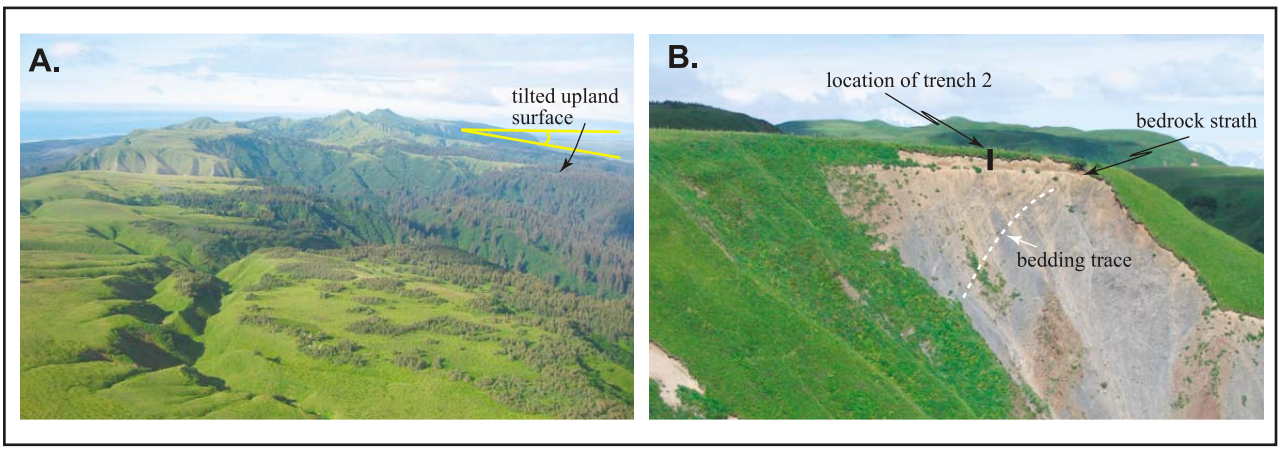

Figure 5. Photographs of the Suckling Hills upland surface. (a) Aerial photograph of the Suckling Hills, looking southwest. The upland surface dips to the right. (b) Photograph of truncated bedrock, erosional strath, and loess deposits. Black bar indicates location of trench 2 and is ~2 m in height. Location of trenches shown in Figure 3b.

marine terrace is deformed by the Suckling Hills Fault. The change in strike of these exposures mirrors that of the open syncline suggesting the Suckling Hills Fault itself may be folded with the open syncline or the fault may have displaced or reactivated a folded surface in the Poul Creek Formation. From geometry alone, the relative timing between the two generations of folds is unclear.

[19] The northeasterly strike of bedding and the axial plane of the anticline in the Suckling Hills are consistent with bedding and fold orientations throughout the western syntaxis (Figure 2). Moreover, the steep northwesterly plunge of the syncline is comparable to fold axes in areas within the syntaxis that have experienced complex deformational overprints [*Bruhn et al.*, 2004; *Pavlis et al.*, 2004]. Finally, the trend and plunge of the axis of the Suckling Hills syncline is comparable to the axis of the monocline on Kayak Island suggesting that these structures may be related to the same generation of deformational events (Figure 3d).

4.4. The Suckling Hills Upland Surface

[20] Similar to the offshore erosional surface at Kayak Island, the Suckling Hills contain a conspicuously flat, upland surface dipping to the northwest (Figures 3, 5, and 6). The Suckling Hills reach a maximum elevation of ~400 m and display a marked topographic asymmetry with a steep escarpment on its eastern flank and a gently dipping western flank that comprises the upland surface (Figures 5a and 6). Structural relief exceeds topographic relief in the Suckling Hills (Figure 3b) and field observations reveal that the upland surface is an erosional surface that cuts bedding at a moderate to high angle (Figure 5b).

[21] To measure the orientation of the upland surface, we used field photos and a slope map derived from DEM data to choose areas of the upland surface not dissected by streams and then extracted subsets of spatial data from the DEM (Figure 6a). We then used a least squares regression to find the best fit plane through the points and estimated error on the dip measurement. Dip of the upland surface varies subtly across the length of the Suckling Hills from 4 to 5 degrees on the northwest side of the Suckling Hills to nearly horizontal on the southeast side closest to the Suckling Hills Fault. The average dip of the upland surface calculated using an average of best fit planes to subsets of the elevation data is 4.1 $\pm$ 0.6 degrees toward 327, which agrees well with the mean elevation profile taken from a 10 km swath across the central Suckling Hills (Figure 6b). This value is used as a representative dip for further calculations.

[22] The erosional surface forms a bedrock strath and is everywhere overlain by ~2m of fine-grained loess. Several test pits and two trenches were dug into the loess deposits to help determine the nature and age of the erosional surface (Figures 3b and 5b). Both trenches contained monotonous sections of silty loess with soil profiles developed within the upper 0.5–1.0 m and an increase in rock fragments within 0.3 m of the bedrock strath. The strath contact is sharp, with a dip of 6 degrees toward 325 in trench 2 and a dip of 5 degrees toward 192 in trench 1 (Figure 3b). At the base of the two trenches, samples were taken for OSL dating. As part of the processing, the samples were wet sieved to 63–180 μm grain size, which removed rock fragments. The ages of the two samples overlap within standard error (Table 1). The weighted mean and standard deviation for the pooled ages is 8.85 $\pm$ 0.81 ka.

[23] The origin of the Suckling Hills upland surface is unknown. Because the Suckling Hills form an isolated topographic high surrounded by glacial outwash plains close to sea level, we think it is unlikely the upland surface formed by fluvial processes. We have examined several marine terraces along the coast including terraces at Cape Suckling, Kayak Island, Wingham Island, and Cape Yakataga, all of which have significant decimeter to meter scale microtopography, differentially weathered beds, cobbles, and assorted marine debris such as shells or wood. Having excavated several test pits, two trenches, and investigated natural exposures, we found the loess-strath contact to be universally planar and without features indicative of a marine

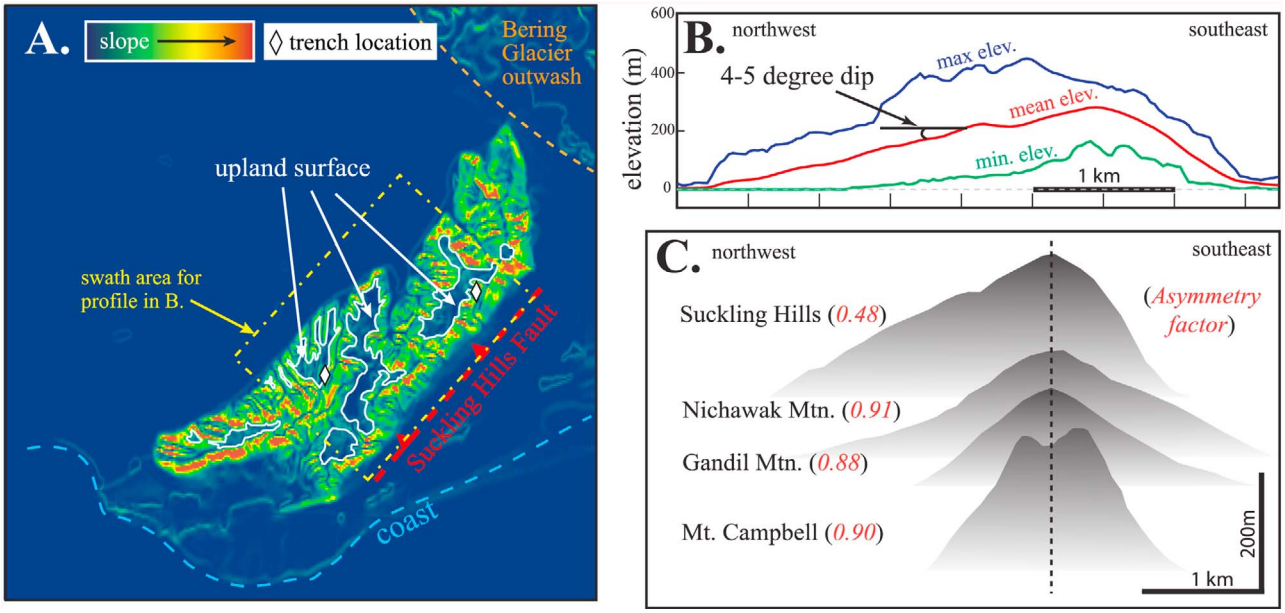

Figure 6. (a) Slope map of the Suckling Hills generated from 15 m DEM data. Blue colors represent low slope. The Suckling Hills erosional surface is outlined in white. (b) Minimum, maximum, and average topographic profiles of the Suckling Hills calculated from a 10 km wide swath, location in Figure 6a. (c) Mean topographic profiles calculated from ~5 km swaths across the short axes of the listed mountain blocks. The asymmetry factor was calculated by drawing a vertical line through the maximum elevation along the mean profile (crest of mountain block) and creating a ratio of the area beneath the profile from either side of this vertical line. Deviations from 1 indicate more pronounced asymmetry. Location of the mountain blocks is shown in Figure 2.

terrace. We have also failed to find any glacial erratics, although we prefer the interpretation that the Suckling Hills were beveled by glacial erosion. Isostatic modeling of ice thickness in the LGM [*Chapman et al.*, 2009] and perched, glacially dammed lacustrine sediments on the flanks of the Suckling Hills [*Fleisher et al.*, 1999] suggest the Suckling Hills were recently overrun by ice and were potentially covered by ice in past glaciations.

[24] The presence of the low-angle, upland erosional surface distinguishes the Suckling Hills from other nearby mountain blocks that were also overridden by the Bering-Stellar glacial system such as Nichawak Mtn., Gandil Mtn., and Mt. Campbell (Figure 2). These mountain blocks exhibit symmetry across their short axes consistent with glacial erosion and development of glacial landforms such as bedrock drumlins or roches moutonnées [*Benn and Evans*, 1998] (Figure 6c). We suggest that the upland surface was rotated in the hanging wall of the Suckling Hills Fault by slip on the fault and that the surface may have originally been sub-horizontal.

[25] As the Bering and Stellar Glaciers flow toward the coast, they coalesce and form piedmont sheet glaciers, which are consistent with sub-horizontal bedrock shields [*Benn and Evans*, 1998]. Rapid retreat of the Bering Glacier in the last century has exposed sub-horizontal substrates and bedrock surfaces near the coast [*Bruhn et al.*, 2010; *Fleisher et al.*, 1998] and similar sub-horizontal surfaces are imaged offshore in the Bering Trough [*Worthington et al.*, 2008; *Berger et al.*, 2008]. Furthermore, the correlation between the dip direction of the upland surface (327) and plunge direction of the fold axis of the syncline (330) in the Suckling Hills, the presence and orientation of the Suckling Hills Fault, the steep escarpment on the eastern flank of the Suckling Hills, and a similar geometry between the Kayak Island offshore surface and Suckling Hills upland surface all suggest to us a potential link between the dip of the upland surface and the Suckling Hills Fault.

[26] The OSL age for the basal loess deposits imply the upland surface was exposed as bare bedrock ~9 ka, consistent with the timing of ice retreat following the LGM

Table 1. Optically Stimulated Luminescence Data

Lab Number	H_2O%	U (ppm)	Th (ppm)	K_2O%	Cosmic Dose Rate[a] (Gy/ka)	De[b] (Gy)	Dose Rate (Gy/ka)	n[c]	OSL Age[b] (ka)
USU-219	17.0 ± 5.1	1.6 ± 0.1	5.4 ± 0.5	1.43 ± 0.04	0.19 ± 0.02	15.05 ± 3.46	1.78 ± 0.09	21(33)	8.47 ± 2.01
USU-220	13.3 ± 4.0	2.3 ± 0.2	5.9 ± 0.5	1.57 ± 0.04	0.20 ± 0.02	18.98 ± 7.24	2.13 ± 0.10	21(53)	8.92 ± 0.89

[a]Calculated from *Prescott and Hutton* [1988] using 1 m sample depth.
[b]Reported to 1σ, for OSL age includes random and systematic errors calculated in quadrature.
[c]Number of accepted aliquots used to calculate mean, total aliquots in parentheses.

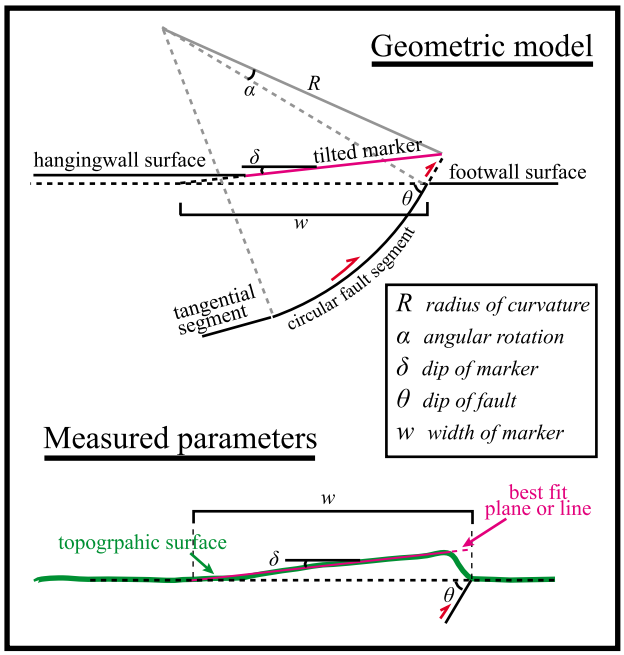

Figure 7. (top) A simplified geometric model for deformation above a listric thrust, adapted from *Amos et al.* [2007]. (bottom) A dimensionless example of a deformed marker, in this case, a tilted topographic surface above a listric thrust, and the parameters measured as inputs into the kinematic model in this study.

(~10 ka) [*Fleisher et al.*, 1999]. This provides a minimum age estimate for the formation of the upland surface, although it is equally possible that the upland surface formed during an older glaciation or from a combination of glacial advances and that the bedrock surface was only stripped of its cover or modified slightly in the LGM.

5. Kinematic Fault Model

[27] To estimate the timing and magnitude of slip on the Suckling Hills Fault and Kayak Island Zone, we employ a fault kinematic model modified from *Amos et al.* [2007] (Figure 7). Strata overlying the Kayak Island Zone offshore surface display increasing dip with depth suggestive of progressive limb rotation throughout the growth of the Kayak Island Zone, including Quaternary growth imaged in the seismic data (Figure 4). Likewise, bedding in the hanging wall of the Suckling Hills Fault dips 60–70 degrees, whereas the upland surface dips only ~4 degrees (Figure 3). A wide variety of fault models can produce progressive limb rotation [*Hardy and Poblet*, 1994; *Suppe et al.*, 2004; *Medwedeff and Suppe*, 1997; *Amos et al.*, 2007], however, models that produce an emergent thrust that breaks the surface as well as progressive limb rotation include shear fault-bend-folding [*Suppe et al.*, 2004] and fault-bend-fold models involving multiple ramps [*Medwedeff and Suppe*, 1997]. Documented examples of shear fault-bend-folds in the Cascadia and Nankai Trough accretionary wedges have backlimb angles a third as steep as fault dip [*Suppe et al.*, 2004]. Cumulative displacements across the Kayak Island Zone and Suckling Hills Fault show steep backlimb dips that equal or exceed the dip of the fault plane in the near surface (Figures 3 and 4). Therefore, we suggest that a fault-bend-fold model with multiple ramps is more appropriate for the Suckling Hills and Kayak Island Zone. In multiple ramp models, as the number of ramps increase, the fault surface becomes increasingly curvilinear as the angle between axial surfaces decreases until the fault approaches a listric geometry such that in the absence of distinct dip panels, a listric fault model is the more robust [*Seeber and Sorlien*, 2000].

[28] Building upon previous models for listric thrusts [*Erslev*, 1986; *Seeber and Sorlien*, 2000], *Amos et al.* [2007] developed a listric thrust model that consists of a circular fault segment and tangential fault ramp at depth where slip $S = R\alpha$, where R is the radius of curvature and α is the angle of rotation in radians (Figure 7). Substituting for R and α, slip can be expressed as

$$S = \{w + [(w/\{\tan[\theta]/C\}) - 1)]\}\delta/\sin(\theta)$$

where,

$$C = \sin(\delta) - \{[1 - \cos(\delta)]/[\tan(\delta)]\}$$

and w, θ, and δ are backlimb width, fault dip, and backlimb dip, respectively. The solution for slip is independent of vertical offset or uplift. Natural listric fault systems are unlikely to contain only circular segments with a higher probability of variable curvature along the fault surface, which would result in concavity or convexity along the backlimb [*Amos et al.*, 2007]. The Suckling Hills upland surface and Kayak Island Zone offshore surface both display a slight convexity, with a decrease in backlimb dip toward the leading fault (Figures 3 and 4). In the listric model, a decrease in backlimb dip is expected with an increase in the radius of curvature (decreasing the fault curvature), which would cause an underestimation of total slip. In our calculations, we discarded subsets of elevation data for the surfaces near the faults, in effect extending a single plane with constant dip to the fault trace, so that it is unlikely we underestimate slip.

[29] Following *Amos et al.* [2007], we use a Monte Carlo approach to calculate uncertainties for slip and slip rate. We list the measured or approximated input parameters for the

Table 2. Monte Carlo Simulation Parameters and Results

	Backlimb Width[a] (m)	Fault Dip[b] (θ)	Backlimb Dip[a] (θ)	Slip (m)	Age (ka)	Slip Rate (mm/yr)
Kayak Island Zone	2500 ± 250	50–70	1.0 ± 0.25	50.6 ± 14.3	14.5 ± 1.1	3.5 ± 1.0
Suckling Hills Fault	3000 ± 500	50–70	4.1 ± 0.6	257 ± 58	55 ± 5;	4.7 ± 1.2;
					140 ± 10;	1.8 ± 0.4;
					1000 ± 100	0.2 ± 0.1

[a]The backlimb corresponds to the tilted erosional surface in each location.
[b]Normal distributions were used for all parameters except fault dip, which was uniformly distributed.

Suckling Hills and the Kayak Island Zone in Table 2. We generated probability distributions for each parameter that we then sampled randomly over 10^5 runs to produce a solution population. For the Suckling Hills, we use a normal distribution of width of the upland surface, with mean and standard deviation values taken from repeated measurements along elevation profiles across the central Suckling Hills. For dip, we use the values and errors associated with the best fit plane through the upland surface. We estimate the dip of the Suckling Hills Fault from bedding relationships and include large uncertainties that are propagated into our final solutions (Table 2). We use a uniform distribution for fault dip to reflect the range of possible values without weighting an average value. For the Kayak Island Zone, we use repeated measurements from the seismic profile to estimate fault dip, dip of the offshore surface, and width of the offshore surface to construct normal distributions for each input parameter (Table 2). To correct for paleotopography that may have existed at Horizon B time, we drew a line connecting the flat-lying portions of the horizon on either side of the Kayak Island Zone (Figure 4). We then flattened the seismic profile on this line using structural modeling software. This procedure reduced the dip of Horizon B to ~1 degree.

[30] To calculate slip rate for the Kayak Island Zone we used a normal distribution centered on 14.5 ka with a standard deviation of 1.1 ka averaged from variations in LGM ages across the region [*Sirkin and Tuthill*, 1987; *Denton*, 1974; *Rymer and Sims*, 1982; *Blaise et al.*, 1990; *Hamilton*, 1994]. For the Suckling Hills, where the upland surface may be related to older glaciations, we ran the Monte Carlo simulation with normal distributions centered on the LGM, the penultimate glaciation (55 ± 5 ka), the next oldest glaciation (140 ± 10 ka), and the Mid-Pleistocene Transition (1000 ± 100 ka) [*Clark et al.*, 2006; *Briner and Kaufman*, 2008] to present a range of possible values. Final calculated uncertainties are reported to one standard deviation (Table 2). For the Kayak Island Zone, we calculate a slip estimate of 50.6 ± 14.3 m and slip rate estimate of 3.5 ± 1.0 mm/yr since the LGM. Our estimate for total slip on the Suckling Hills Fault is 257 ± 59 m with estimated slip rates of 18 ± 4 mm/yr for the LGM, 4.7 ± 1.2 mm/yr for the penultimate glaciation, 1.8 ± 0.4 mm/yr for the ~140 ka glaciation, and 0.2 ± 0.1 mm/yr for the Mid-Pleistocene Transition, which we consider a minimum end-member.

6. Discussion

6.1. Pleistocene Fault Activity

[31] The maximum slip rate estimate for the Suckling Hills Fault is 18 ± 4 mm/yr, which is significantly higher than slip rate estimates for the Kayak Island Zone and would indicate that the Suckling Hills Fault accommodates a quarter of the total horizontal shortening for the Yakutat microplate. This rate is also disproportionate to other active fault zones such as the Pamplona Zone that forms the offshore deformation front (Figure 1) and have convergence rate estimates of 6–10 mm/yr [*Worthington et al.*, 2010; *Chapman et al.*, 2008]. We therefore speculate that the Suckling Hills upland surface may have formed prior to the LGM and treat this high rate with suspicion. Our slip rate estimates calculated using the penultimate and ~140 ka glaciation are broadly comparable to the slip rates estimated for the Kayak Island Zone, however, we stress that these too may be overestimates if our assumption of an originally sub-horizontal erosional surface is incorrect. Slip rate estimates for the Suckling Hills Fault remain poorly constrained at < ~5 mm/yr.

[32] Slip rate estimates for the Kayak Island Zone are higher in the kinematic fault model (3.5 ± 1.0 mm/yr) than calculations based on offset of Horizon B across the small scarp in the seismic profile (~2.4 mm/yr). The results of the fault model are largely dependent on the width and dip of the erosional surface and independent of elevation or offset across the scarp. Complexities not addressed in our fault model include differential compaction [*Carminati and Santantonio*, 2005] and variable paleotopography, which may result in an overestimate of slip in the kinematic model. Complexities such as near-surface fault deflections and unseen deformation within the scarp area may result in an underestimate of slip for the calculation based solely on vertical offset.

6.2. Insight Into the Accretion of the Yakutat Microplate

[33] The presence of active slip along the Suckling Hills Fault and Kayak Island Zone helps to reduce an unresolved slip rate deficit across the orogen [*Pavlis et al.*, 2004; *Chapman et al.*, 2008; *Worthington et al.*, 2010] and establishes these structures as among the most recently active within the western syntaxis region. The geometry and orientation of the Suckling Hills Fault and Kayak Island Zone are comparable to each other as well as the Bering Glacier structure to the north [*Bruhn et al.*, 2010; *Doser et al.*, 2007]. All of these structures appear to be northwest-dipping thrust faults, located along strike from one another, that are oriented approximately perpendicular to present Yakutat microplate motion [*Elliott et al.*, 2010]. In addition, the Bering Glacier structure, Kayak Island Zone, and Suckling Hills Fault all separate multiply deformed rocks of the western syntaxis from the central YFTB. As a result, we suggest that these faults form a single fault system for >100 km along the eastern edge of the western syntaxis. These faults may currently form a disconnected fault system that is in the process of linking by lateral fault growth.

[34] The YFTB expanded southward throughout the Neogene with increased net convergence [*Plafker*, 1987]. Evidence for this progression comes from offshore compressional structures east of the Kayak Island Zone that offset progressively younger strata leading up to the Pamplona Zone [*Bruns and Schwab*, 1983] and the fan-like geometry of the offshore YFTB [*Plafker*, 1987] (Figure 1). Also during the Neogene, the Yakutat microplate included a component of westward translation during oblique subduction along the North American plate margin [*Pavlis et al.*, 2004]. Accretion at the western end of the Yakutat microplate has resulted in oroclinal bending, complex deformational overprints, and multiple generations of folds in what is now the western syntaxis [*Pavlis et al.*, 2004; *Bruhn et al.*, 2004; *Pavlis and Bruhn*, 2011]. We propose that the structures of the central YFTB became unfavorably oriented for continued shortening, with respect to Yakutat microplate motion, once they were translated into the western syntaxial corner (Figure 8).

[35] At the eastern end of the YFTB, the active Malaspina Fault strikes 065 to 075 degrees [*Plafker et al.*, 1994], perpendicular to the direction of Yakutat microplate motion at

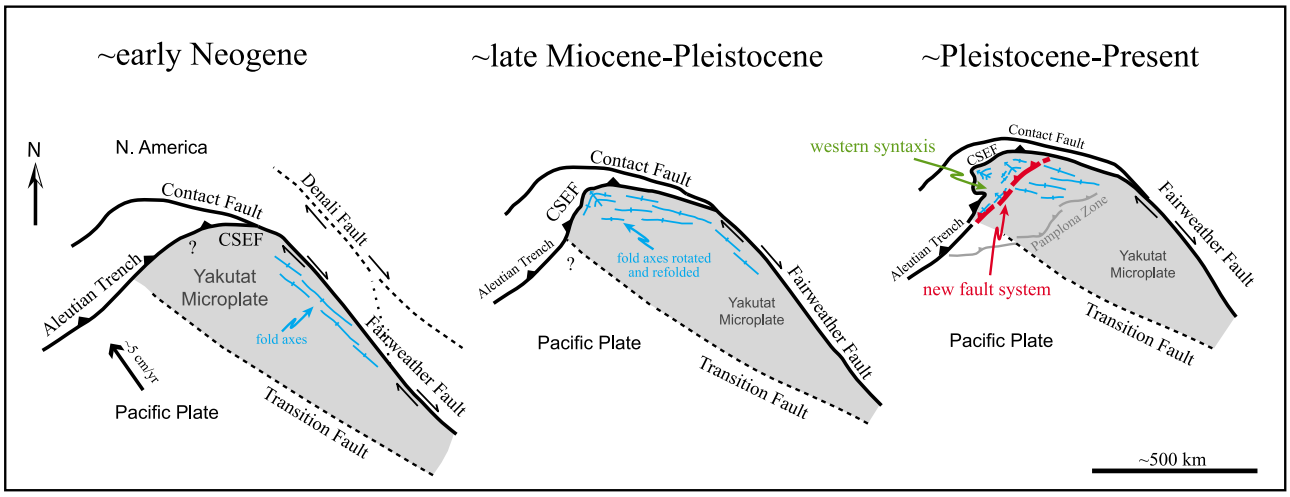

Figure 8. A series of schematic drawings illustrating the proposed tectonic evolution of the western syntaxis in the Yakutat microplate. Oblique subduction of the Yakutat microplate in the early Neogene resulted in slip-partitioned deformation that created fold and thrust structures, oriented sub-parallel to the microplate margin. With continued subduction, these structures were translated westward toward the intersection of the Aleutian Trench and the south Alaska margin that form a geometric corner. In the late Miocene to Pleistocene, the previously margin-parallel structures were rotated and refolded within the corner as the sedimentary cover was accreted, forming the western syntaxis of the Yakutat microplate. As a result of this deformation and ongoing accretion, the structures in the western Yakutat microplate became unfavorably oriented for continued deformation and a new fault system developed seaward of the refolded structures. The new fault system trends into the Aleutian Trench and straightened the western syntaxis margin.

~337 degrees [*Elliott et al.*, 2010]. Moving westward in the central YFTB, thrust faults become increasingly oblique to microplate motion [*Chapman et al.*, 2008]. Thrust faults just east of the Bering Glacier, strike 090 to 095 degrees, the axis of the overturned monocline exposed on Kayak Island plunges toward 144, and the axis of the syncline in the Suckling Hills plunges toward 330 (Figures 2 and 3). In contrast, thrust faults exposed on Kayak Island strike ~045 degrees, the axis of the anticline in the Suckling Hills trends ~060 degrees, and the upper reaches of the Bering Glacier trend 070 to 075 degrees (Figures 2 and 3), all subperpendicular to the direction of Yakutat microplate motion and along strike from the trace of the Aleutian Trench (Figure 1).

[36] We propose that, as a result of deformational overprints, complex refolding, and rotation within the incipient western syntaxis [*Bruhn et al.*, 2004; *Pavlis et al.*, 2004; *Pavlis and Bruhn*, 2011], the Kayak Island Zone, Suckling Hills Fault, and Bering Glacier structure formed a new fault system that cut across the orogen and straightened the western syntaxis margin (Figure 8). This new fault system may form the onshore extension of the Aleutian Trench. Increasing structural complexity within the western syntaxis suggests to us that some of the earliest rocks to be accreted to Southern Alaska from the Yakutat microplate are now located within the core of the western syntaxis. The development of the new fault system may represent an advanced stage of accretion in which the rocks in the western syntaxis, west of the new fault system, are in the process of becoming fully accreted to the south Alaska margin.

[37] The structural evolution of the western syntaxis in the Yakutat microplate may provide a template for understanding the process of accretion in other modern or ancient oblique convergent margins. Diagnostic features of the St. Elias orogen and YFTB include significant changes in structural style along strike, increasing structural complexity in the direction of lateral transport, multiple generations of deformation along with associated structural overprints, and temporal changes structural reorganization with continued accretion.

[38] Of these features, the interplay between structural organization and the stage of accretion has implications for understanding changes in the pattern of deformation through time in oblique convergent margins. One implication is that the geometry and composition of the backstop evolves with prolonged accretion. As material is accreted to the margin in a syntaxis or corner, the mechanical rigidity, taper, and dip direction of the backstop may change, which in turn may affect deformation patterns within the accretionary wedge [*Byrne et al.*, 1993].

7. Conclusions

[39] The Suckling Hills and Kayak Island preserve subplanar erosional surfaces that were likely cut by glacial erosion in the Pleistocene. We suggest that these surfaces were created during the LGM (~14.5 ka), however, the Suckling Hills surface could be as old as the Mid-Pleistocene Transition (0.7–1 Ma). These surfaces were subsequently tilted in the hanging wall of west-dipping thrust faults including the Suckling Hills Fault and faults within the Kayak Island Zone as imaged in seismic data. Using a geometric model from *Amos et al.* [2007] that relates angular rotation to the amount of slip on a listric thrust, we estimated slip rates using a Monte Carlo approach. We estimate that the Kayak Island Zone has a slip rate of 3.5 ± 1.0 mm/yr since the LGM.

We estimate that the Suckling Hills Fault has as a slip rate of < ~5 mm/yr.

[40] The Suckling Hills Fault and Kayak Island Zone lie at the easternmost extent of complex deformational overprints in the western syntaxis and together with the Bering Glacier structure to the north, form a fault network and structural domain boundary that crosses the width of the St. Elias orogen. Structural relationships observed at Kayak Island and in the Suckling Hills suggest that folds of the central Yakataga Fold and Thrust Belt (YFTB) were translated westward into an incipient syntaxis were they were refolded and rotated within an orogenic corner. As a result, these older structures were no longer favorably oriented with respect to Yakutat microplate motion for continued shortening. We propose that the fault system consisting of the Kayak Island Zone, Suckling Hills Fault, and Bering Glacier structure represents a new structural boundary that effectively straightened and realigned the western syntaxis margin (Figure 8). This boundary forms the northeastern extension of the Aleutian Trench in the Yakutat microplate. Progressive structural overprinting with changing orientations as deformation evolves through time may be a signature of orogenic corners in oblique convergent margins.

[41] **Acknowledgments.** This research was supported by the St. Elias erosion and tectonics project (STEEP) through NSF grants EAR0409009 to T. Pavlis, EAR0408959 to R. Bruhn, and EAR 0408584 to S. Gulick. Seismic acquisition was supported by NSF grant OCE0351620 to S. Gulick. We are grateful to Michael Vorkink for assistance in the field and to Tammy Rittenour for OSL dating. Reviews by A. Meigs, H. Kelsey, and P. Umhoefer significantly improved the manuscript. This is UTIG contribution #2427.

References

Amos, C. B., D. W. Burbank, D. C. Nobes, and S. A. L. Read (2007), Geomorphic constraints on listric faulting: Implications for active deformation in the Mackenzie Basin, South Island, New Zealand, *J. Geophys. Res.*, *112*, B03S11, doi:10.1029/2006JB004291.

Begét, J. E. (2001), Continuous Late Quaternary proxy climate records from loess in Beringia, *Quat. Sci. Rev.*, *20*, 499–507, doi:10.1016/S0277-3791(00)00102-5.

Benn, D. I., and D. J. A. Evans (1998), *Glaciers and Glaciation*, Arnold, London.

Berger, A. L., and J. A. Spotila (2008), Denudation and deformation in a glaciated orogenic wedge: The St. Elias orogen, Alaska, *Geology*, *36*, 523–526, doi:10.1130/G24883A.1.

Berger, A. L., S. P. S. Gulick, J. A. Spotila, J. M. Jaeger, J. B. Chapman, L. A. Lowe, T. L. Pavlis, K. R. Ridgway, B. A. Willems, and R. McAleer (2008), Quaternary Tectonic Response to Intensified Glacial Erosion in an Orogenic Wedge, *Nat. Geosci.*, *1*, 793–799, doi:10.1038/ngeo334.

Blaise, B., J. J. Clague, and R. W. Mathewes (1990), Time of maximum Late Wisconsin glaciation, west coast of Canada, *Quat. Res.*, *34*, 282–295, doi:10.1016/0033-5894(90)90041-I.

Briner, J. P., and D. S. Kaufman (2008), Late Pleistocene mountain glaciation in Alaska: Key chronologies, *J. Quat. Sci.*, *23*, 659–670, doi:10.1002/jqs.1196.

Brocher, T. M., G. S. Fuis, M. A. Fisher, G. Plafker, and M. J. Moses (1994), Mapping the megathrust beneath the northern Gulf of Alaska using wide-angle seismic data, *J. Geophys. Res.*, *99*(B6), 11,663–11,685, doi:10.1029/94JB00111.

Bruhn, R. L., T. L. Pavlis, G. Plafker, and L. Serpa (2004), Deformation during terrane accretion in the Saint Elias orogen, Alaska, *Geol. Soc. Am. Bull.*, *116*, 771–787, doi:10.1130/B25182.1.

Bruhn, R. L., R. Forster, A. L. J. Ford, T. L. Pavlis, and M. Vorkink (2010), Structural geology and glacier dynamics, Bering and Steller Glaciers, Alaska, in *Bering Glacier: Interdisciplinary Studies of Earth's Largest Temperate Surging Glacier*, edited by R. A. Shuchman and E. G. Josberger, *Spec. Pap. Geol. Soc. Am.*, *462*, 217–233, doi:10.1130/2010.2462(11).

Bruns, T. R., and W. C. Schwab (1983), Structure maps and seismic stratigraphy of the Yakataga segment of the continental margin, northern Gulf of Alaska, *Misc. Field Stud. Map MF-1424*, 4 sheets, scale 1:250,000, U.S. Geol. Surv., Reston, Va.

Byrne, D. E., W. Wang, and D. M. Davis (1993), Mechanical role of backstops in the growth of forearcs, *Tectonics*, *12*(1), 123–144, doi:10.1029/92TC00618.

Carlson, P. R., and B. F. Molnia (1975), Preliminary isopach map of Holocene sediments, northern Gulf of Alaska, *U. S. Geol. Surv. Open File Rep. 75–507*, 1 sheet, scale 1:500,000, U.S. Geol. Surv., Reston, Va.

Carminati, E., and M. Santantonio (2005), Control of differential compaction on the geometry of sediments onlapping paleoescarpments: Insights from field geology (Central Apennines, Italy) and numerical modeling, *Geology*, *33*, 353–356, doi:10.1130/G21262.1.

Chapman, J. B., et al. (2008), Neotectonics of the Yakutat collision: Changes in deformation driven by mass redistribution, in *Active Tectonics and Seismic Potential of Alaska*, *Geophys. Monogr. Ser*, vol. 179, edited by J. T. Freymueller et al., pp. 65–81, AGU, Washington, D. C., doi:10.1029/179GM04.

Chapman, J. B., P. J. Haeussler, and T. L. Pavlis (2009), Quaternary uplift history of Wingham Island, south-central Alaska, *U.S. Geol. Surv. Prof. Paper*, *1760–B*, 13 pp.

Christeson, G. L., S. P. Gulick, H. J. van Avendonk, L. L. Worthington, R. S. Reece, and T. L. Pavlis (2010), The Yakutat terrane: Dramatic change in crustal thickness across the Transition Fault, Alaska, *Geology*, *38*, 895–898, doi:10.1130/G31170.1.

Clark, P. U., D. Archer, D. Pollard, J. D. Blum, J. A. Rial, V. Brovkin, A. C. Mix, N. C. Pisias, and M. Roy (2006), The middle Pleistocene transition: Characteristics, mechanisms, and implications for long-term changes in atmospheric pCO_2, *Quat. Sci. Rev.*, *25*, 3150–3184, doi:10.1016/j.quascirev.2006.07.008.

Denton, G. H. (1974), Quaternary glaciations of the White River valley, Alaska, with a regional synthesis for the northern St. Elias mountains, Alaska and Yukon Territory, *Geol. Soc. Am. Bull.*, *85*, 871–892, doi:10.1130/0016-7606(1974)85<871:QGOTWR>2.0.CO;2.

Doser, D. I., K. R. Wiest, and J. M. Sauber (2007), Seismicity of the Bering Glacier region and its relation to tectonic and glacial processes, *Tectonophysics*, *439*, 119–127, doi:10.1016/j.tecto.2007.04.005.

Eberhart-Phillips, D., D. H. Christensen, T. M. Brocher, R. Hansen, N. A. Ruppert, P. J. Haeussler, and G. A. Abers (2006), Imaging the transition from Aleutian subduction to Yakutat collision in central Alaska, with local earthquakes and active source data, *J. Geophys. Res.*, *111*, B11303, doi:10.1029/2005JB004240.

Elliott, J. L., C. F. Larsen, J. T. Freymueller, and R. J. Motyka (2010), Tectonic block motion and glacial isostatic adjustment in southeast Alaska and adjacent Canada constrained by GPS measurements, *J. Geophys. Res.*, *115*, B09407, doi:10.1029/2009JB007139.

Erslev, E. (1986), Basement balancing of Rocky Mountain foreland uplifts, *Geology*, *14*, 259–262, doi:10.1130/0091-7613(1986)14<259:BBORMF>2.0.CO;2.

Fleisher, P. J., D. H. Cadwell, and E. H. Mueller (1998), Tsivat Basin Conduit System Persists through two surges, Bering Piedmont Glacier, Alaska, *Geol. Soc. Am. Bull.*, *110*, 877–887, doi:10.1130/0016-7606(1998)110<0877:TBCSPT>2.3.CO;2.

Fleisher, P. J., E. H. Muller, D. H. Peteet, and M. S. Lachniet (1999), Arctic enigma: Was Alaska's Late Pleistocene Bering Glacier really out of step with its neighbors?, *Geotimes*, *44*(1), 16–21.

Griscom, A., and P. E. Sauer (1990), Interpretation of magnetic maps of the northern Gulf of Alaska, with emphasis on the source of the slope anomaly, *Open File Rep.*, *90–348*, 19 pp.

Hamilton, T. D. (1994), Late Cenozoic glaciation of Alaska, in *The Geology of Alaska*, vol. G-1, *The Geology of North America*, edited by G. Plafker and H. C. Berg, pp. 813–844, Geol. Soc. of Am., Boulder, Colo.

Hardy, S., and J. Poblet (1994), Geometric and numerical model of progressive limb rotation in detachment folds, *Geology*, *22*, 371–374, doi:10.1130/0091-7613(1994)022<0371:GANMOP>2.3.CO;2.

Jaeger, J. M., C. A. Nitrouer, N. D. Scott, and J. D. Milliman (1998), Sediment accumulation along a glacially impacted mountainous coastline: North-east Gulf of Alaska, *Basin Res.*, *10*, 155–173, doi:10.1046/j.1365-2117.1998.00059.x.

Lagoe, M. B., C. H. Eyles, N. Eyles, and C. Hale (1993), Timing of late Cenozoic tidewater glaciation in the far north Pacific, *Geol. Soc. Am. Bull.*, *105*, 1542–1560, doi:10.1130/0016-7606(1993)105<1542:TOLCTG>2.3.CO;2.

Mazzotti, S., and R. D. Hyndman (2002), Yakutat collision and strain transfer across the northern Canadian Cordillera, *Geology*, *30*, 495–498, doi:10.1130/0091-7613(2002)030<0495:YCASTA>2.0.CO;2.

Medwedeff, D. A., and J. Suppe (1997), Multibend fault-bend folding, *J. Struct. Geol.*, *19*, 279–292, doi:10.1016/S0191-8141(97)83026-X.

Meigs, A., S. Johnston, J. Garver, and J. Spotila (2008), Crustal-scale structural architecture, shortening, and exhumation of an active eroding orogenic wedge (the Chugach/St. Elias Range, southern Alaska), *Tectonics*, *27*, TC4003, doi:10.1029/2007TC002168.

Miller, D. J. (1961), Geology of the Katalla district, Gulf of Alaska Tertiary Province, Alaska, *U.S. Geol. Surv. Open File Rep. 61–99*, 2 sheets, scale 1:96,000, U.S. Geol. Surv., Reston, Va.

Miller, D. J. (1975), Geologic map and sections of central part of the Katalla District, Alaska, *Misc. Field Stud. Map 722*, 2 sheets, scale 1:40,000, U.S. Geol. Surv., Reston, Va.

Pavlis, T. L., and R. L. Bruhn (2011), Application of LIDAR to resolving bedrock structure in areas of poor exposure: An example from the STEEP study area, southern Alaska, *Geol. Soc. Am. Bull.*, *123*, 206–217, doi:10.1130/B30132.1.

Pavlis, T. L., C. Picornell, L. Serpa, R. L. Bruhn, and G. Plafker (2004), Tectonic processes during oblique collision: Insights from the St. Elias Orogen, northern North American Cordillera, *Tectonics*, *23*, TC3001, doi:10.1029/2003TC001557.

Plafker, G. (1969), Tectonics of the March 27, 1964, Alaska earthquake, *U. S. Geol. Surv. Prof. Pap.*, *543-I*, 74 pp.

Plafker, G. (1974), Preliminary geologic map of Kayak and Wingham Islands, Alaska, *U.S. Geol. Surv. Open File Rep. OF 74–82*, 1 sheet, scale 1:31,680, U.S. Geol. Surv., Reston, Va.

Plafker, G. (1987), Regional geology and petroleum potential of the northern Gulf of Alaska, in *Geology and Resource Potential of the Continental Margin of the Western North American and Adjacent Ocean Basins—Beaufort Sea to Baja California*, *Earth Sci. Ser.*, vol. 6, edited by D. W. Scholle, A. Grantz, and J. G. Vedder, pp. 229–268, Circum-Pac. Counc. for Energy and Miner. Resour., Menlo Park, Calif.

Plafker, G., and W. O. Addicott (1976), Glaciomarine deposits of Miocene through Holocene age in the Yakataga Formation along the Gulf of Alaska margin, Alaska, *U.S. Geol. Surv. Open File Rep.*, *76–84*, 36 pp.

Plafker, G., J. C. Moore, and G. R. Winkler (1994), Geology of the southern Alaska margin, in *The Geology of Alaska*, vol. G-1, *The Geology of North America*, edited by G. Plafker and H. C. Berg, pp. 389–449, Geol. Soc. of Am., Boulder, Colo.

Prescott, J. R., and J. T. Hutton (1988), Cosmic ray and gamma ray dosimetry for TL and ESR, *Nucl. Tracks Radiat. Meas.*, *14*, 223–227, doi:10.1016/1359-0189(88)90069-6.

Richter, D. H., C. C. Preller, K. A. Labay, and N. B. Shew (2005), Geologic map of the Wrangell-Saint Elias National Park and Preserve, Alaska, *U.S. Geol. Surv. Sci. Invest. Ser. Map SIM-2877*, U.S. Geol. Surv., Reston, Va.

Rittenour, T. M., R. J. Goble, and M. D. Blum (2005), Development of an OSL chronology for Late Pleistocene channel belts in the lower Mississippi valley, USA, *Quat. Sci. Rev.*, *24*, 2539–2554, doi:10.1016/j.quascirev.2005.03.011.

Rymer, M. J., and J. D. Sims (1982), Lake-sediment evidence for the date of deglaciation of the Hidden Lake area, Kenai Peninsula, Alaska, *Geology*, *10*, 314–316, doi:10.1130/0091-7613(1982)10<314:LEFTDO>2.0.CO;2.

Seeber, L., and C. C. Sorlien (2000), Listric thrusts in the western Transverse Ranges, California, *Geol. Soc. Am. Bull.*, *112*, 1067–1079, doi:10.1130/0016-7606(2000)112<1067:LTITWT>2.0.CO;2.

Sirkin, L., and S. J. Tuthill (1987), Late Pleistocene and Holocene deglaciation and environments of the southern Chugach Mountains, Alaska, *Geol. Soc. Am. Bull.*, *99*, 376–384, doi:10.1130/0016-7606(1987)99<376:LPAHDA>2.0.CO;2.

Suppe, J., C. D. Connors, and Y. Zhang (2004), Shear fault-bend folding, in *Thrust Tectonics and Hydrocarbon Systems*, edited by K. R. McClay, *AAPG Mem.*, *82*, 303–323.

Worthington, L. L., S. P. Gulick, and T. L. Pavlis (2008), Identifying active structures in the Kayak Island and Pamplona Zone: Implications for offshore tectonics of the Yakutat microplate, Gulf of Alaska, in *Active Tectonics and Seismic Potential of Alaska*, *Geophys. Monogr. Ser*, vol. 179, edited by J. T. Freymueller et al., pp. 257–268, AGU, Washington, D. C., doi:10.1029/179GM14.

Worthington, L. L., S. P. Gulick, and T. L. Pavlis (2010), Coupled stratigraphic and structural evolution of a glaciated orogenic wedge, offshore St. Elias Orogen, Alaska, *Tectonics*, *29*, TC6013, doi:10.1029/2010TC002723.

Zellers, S. D. (1995), Foraminiferal sequence biostratigraphy and seismic stratigraphy of a tectonically active margin; the Yakataga Formation, northeastern Gulf of Alaska, *Mar. Micropaleontol.*, *26*, 255–271, doi:10.1016/0377-8398(95)00031-3.

R. L. Bruhn, Department of Geology and Geophysics, University of Utah, 115 S. 1460 E, Salt Lake City, UT 84112, USA. (ron.bruhn@utah.edu)

J. B. Chapman, SandRidge Energy, 123 Robert S. Kerr Ave., Oklahoma City, OK 73102, USA. (jchapman@sandridgeenergy.com)

S. P. Gulick, Institute for Geophysics, University of Texas at Austin, J.J. Pickle Research Campus, Bldg. 196, 10100 Burnet Rd. (R2200), Austin, TX 78758, USA. (sean@utig.ig.utexas.edu)

T. L. Pavlis, Department of Geological Sciences, University of Texas at El Paso, 500 W. University Blvd., El Paso, TX 79968, USA. (tlpavlis@utep.edu)

L. L. Worthington, Department of Geology and Geophysics, Texas A&M University, MS 3115, College Station, TX 77843, USA. (l.worthington@tamu.edu)